Synchronization by elastic neuronal latencies

Roni Vardi,[1] Reut Timor,[2] Shimon Marom,[3] Moshe Abeles,[1] and Ido Kanter[1,2]

[1]*Gonda Interdisciplinary Brain Research Center, and the Goodman Faculty of Life Sciences, Bar-Ilan University, Ramat-Gan 52900, Israel*

[2]*Deptartment of Physics, Bar-Ilan University, Ramat-Gan 52900, Israel*

[3]*Network Biology Research Laboratories, Technion–Israel Institute of Technology, Haifa 32000, Israel*

(Received 6 August 2012; revised manuscript received 11 December 2012; published 29 January 2013)

Psychological and physiological considerations entail that formation and functionality of neuronal cell assemblies depend upon synchronized repeated activation such as zero-lag synchronization. Several mechanisms for the emergence of this phenomenon have been suggested, including the global network quantity, the greatest common divisor of neuronal circuit delay loops. However, they require strict biological prerequisites such as precisely matched delays and connectivity, and synchronization is represented as a stationary mode of activity instead of a transient phenomenon. Here we show that the unavoidable increase in neuronal response latency to ongoing stimulation serves as a nonuniform gradual stretching of neuronal circuit delay loops. This apparent nuisance is revealed to be an essential mechanism in various types of neuronal time controllers, where synchronization emerges as a transient phenomenon and without predefined precisely matched synaptic delays. These findings are described in an experimental procedure where conditioned stimulations were enforced on a circuit of neurons embedded within a large-scale network of cortical cells *in vitro*, and are corroborated and extended by simulations of circuits composed of Hodgkin-Huxley neurons with time-dependent latencies. These findings announce a cortical time scale for time controllers based on tens of microseconds stretching of neuronal circuit delay loops per spike. They call for a reexamination of the role of the temporal periodic mode in brain functionality using advanced *in vitro* and *in vivo* experiments.

DOI: 10.1103/PhysRevE.87.012724 PACS number(s): 84.35.+i, 87.19.lo, 87.18.Sn

I. INTRODUCTION

Psychological and physiological considerations entail that formation and functionality of neuronal cell assemblies [1–3] depend upon synchronized repeated activation such as zero-lag synchronization [4–6]. Several mechanisms for the emergence of this phenomenon have been suggested [7,8], including the global network quantity, the greatest common divisor of neuronal circuit delay loops [9,10]. This rule captures the interplay between topology, the greatest common divisor (GCD) of circuit loops, and the reverberating mode of activity which is exemplified in Fig. 1. We recently applied a semisynthetic experimental approach using a conditioned stimulation procedure to the study of reverberating Hebbian objects (RHOs) in a physiologically controlled setting. We generated RHOs by stimulations of a subset of neurons embedded in a neural network. This subset was artificially connected to form a local circuit with predefined programmable connectivity and time delays [10]. We found that the observed periodic modes of a given circuit topology were determined by a simple and mechanistically tenable global network quantity—the greatest common divisor of embedded circuit loops. However, they require strict biological prerequisites such as precisely matched delays and connectivity, and synchronization is represented as a stationary mode of activity instead of a transient phenomenon [11,12].

Similarly, the harmonic activity of interconnected computational and communication devices requires accurate specifications, reliable units, and precise wiring. Recently, these demands have been found to apply as well to the emergence of synchronous activity in other networks of threshold elements such as coupled laser networks [13–16]. Viewed from this perspective and given the compromised reliability of their building blocks, the capacity of biological neural networks to generate functional synchronizations is puzzling.

We present in this paper theoretical evidence corroborated experimentally to show how the apparent variability in brain building blocks can turn into an advantage. We show that the unavoidable increase in neuronal response latency [17–19] to ongoing stimulation serves as a nonuniform gradual stretching of neuronal circuit delay loops. This apparent nuisance is revealed to be an essential mechanism in various types of neuronal timers since the emergence of synchronization emerges as a transient phenomenon and without predefined precisely matched synaptic delays. These findings are described in an experimental procedure where conditioned stimulations [10] were enforced on a circuit of neurons embedded within a large-scale network of cortical cells *in vitro* [10,20–22], and are corroborated and extended by simulations of circuits composed of Hodgkin-Huxley (HH) neurons [23,24] with time-dependent latencies. These findings extend in more detail the results of [25] and especially the experimental setup and announce a cortical time scale based on tens of microseconds stretching of neuronal circuit delay loops per spike.

II. NEURONAL RESPONSE LATENCY

At the single neuron level, the most significant feature that appears to work against the formation of synchronies is the tendency of neurons, when stimulated repeatedly, to gradually change their stimulus-response delay over a few milliseconds [17,18]. To exemplify this neuronal feature, experiments were conducted on cultured cortical neurons that were functionally isolated from their network by a pharmacological block of both glutamatergic and GABAergic synapses [18,20] (see Methods section). Schematic of a neuron stimulated every 100 ms from

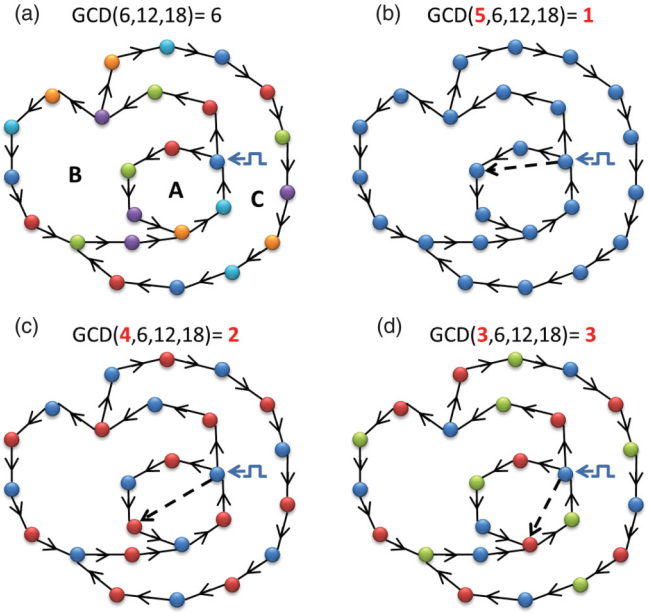

FIG. 1. (Color online) The nonlocal role of the GCD is exemplified by the above figure where a circuit consists of 25 excitable nodes and three loops with total delays of 6τ, 12τ, and 18τ (boundaries of areas A, A + B, and C, respectively, where τ is a unit delay between two connected nodes), and a stimulus to one node. (a) Nodes split into 6-clusters following the GCD(6,12,18) = 6 where nodes belonging to the same cluster are in ZLS. (b) With an additional unidirectional connection (dashed arrow) generating a loop of 5τ, the GCD(5,6,12,18) = 1 and the circuit is in ZLS. (c) An additional loop of 4τ as in (b), where GCD(4,6,12,18) = 2 and the circuit is in 2-clusters. (d) An additional loop of 3τ as in (b), where GCD(3,6,12,18) = 3 and the circuit is in 3-clusters.

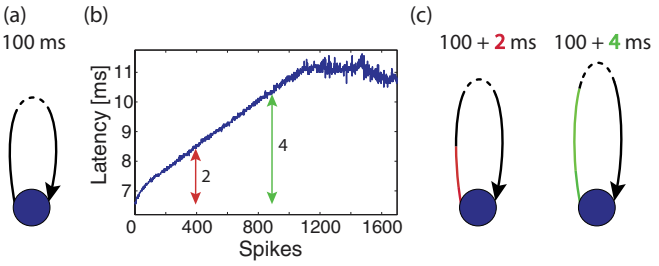

FIG. 2. (Color online) (a) Schematic of a neuron stimulated every 100 ms from the detection of its evoked spike. (b) Experimental results for a neuronal response latency of 2(a) calculated at a time resolution of 1/16 ms (the type of stimulation is given in the Methods section in Ref. [25]). The latency increases by ∼4 ms in ∼100 s (on the average, an increase of ∼4 μs per spike), until the neuron enters the intermittent phase. The serial spike number where latency increases by ∼2 ms (red) and ∼4 ms (green) is labeled. (c) Schematic showing how the increase in the neuronal response latency shown in Fig. 2(b) can also be attributed to the extension of the self-feedback delay while the neuronal response latency remains unchanged.

the detection of its evoked spike is depicted in Fig. 2(a). Figure 2(b) depicts the experimental results for the neuronal response latency, the time lag between stimulation and evoked spike. Results indicate that the latency increases by ∼4 ms in ∼100 s until critical latency is reached, where the neuron enters the intermittent phase [18], characterized by fluctuations of the latency around an average value. The average increment of the latency per spike is ∼4 μs, which represents a finer time scale of cortical dynamics. The increase in the neuronal latency (internal dynamic) can be equivalently attributed to an increase in the time lag between consecutive stimulations whereas the neuronal response latency remains unchanged. For instance, the increase of ∼2 ms in the neuronal latency after ∼400 spikes is equivalent to the scenario where the neuronal response latency is unchanged and the time gap between consecutive stimulations is extended to 100 + 2 ms [Fig. 2(c)]. While the precise underlying mechanisms might be system specific (types of ionic channels and spatial considerations), it is generally agreed that the increase in latency reflects a decline in the exciting conductance and is fully reversible [17,18].

III. NEURONAL RESPONSE LATENCY—CIRCUIT LEVEL

A. First timer—momentary synchronization

To analyze the impact of dynamic neuronal response latency at the circuit level, we artificially generated conditioned stimulations of a circuit of neurons embedded within a large-scale network of cortical cells *in vitro* (see Methods section). Our first experimental design consisted of three neurons forming a heterogeneous neuronal circuit [Fig. 3(a)], where the dynamics is initiated by an electrical stimulation to neuron A only [10]. Conditioned stimulations were given according to the connectivity of the circuit, e.g., conditioned to evoked spike from neuron B, neurons A and C are stimulated after τ ms. One can verify that the circuit [Fig. 3(a)] consists of a 2τ loop (A→B→A) and a 5τ loop (A→B→C→A). Since the greatest common divisor GCD(2,5) = 1, neuronal activity relaxes to zero-lag synchronization (ZLS) as was theoretically predicted [9,14]. Indeed, standard simulations of such a circuit composed of Hodgkin-Huxley neurons [9,10] indicate that after a short transient of 7τ ms ZLS is achieved [Fig. 3(b)]. The parameters used in the Hodgkin-Huxley simulations are detailed in Sec. V A.

A slightly modified circuit is presented in Fig. 3(c) with 2τ and $5\tau + \varepsilon$ loops where ZLS is no longer a solution. Assume that the increase in the neuronal latency per spike, Δ, is independent of the current latency [e.g., a linear fit up to ∼1100 spikes in Fig. 2(b)]. After q evoked spikes per neuron, the effective delay loops are

$$2\tau + 2q\Delta, \quad 5\tau + \varepsilon + 3q\Delta, \tag{1}$$

where the stretching of each unidirectional delay is illustrated by a red thicker bar [Fig. 3(d)]. To verify whether the ratio 2:5 between the two loops is restored the equation below is applied:

$$\frac{2\tau + 2q\Delta}{2} = \frac{5\tau + \varepsilon + 3q\Delta}{5}, \tag{2}$$

which indicates that after

$$q = \frac{\varepsilon}{2\Delta} \tag{3}$$

spikes per neuron ZLS is temporarily restored. Quantitative simulations of such a circuit model composed of Hodgkin-Huxley (HH) neurons with $\Delta = 0.004$ ms, $\varepsilon = 3$ ms and

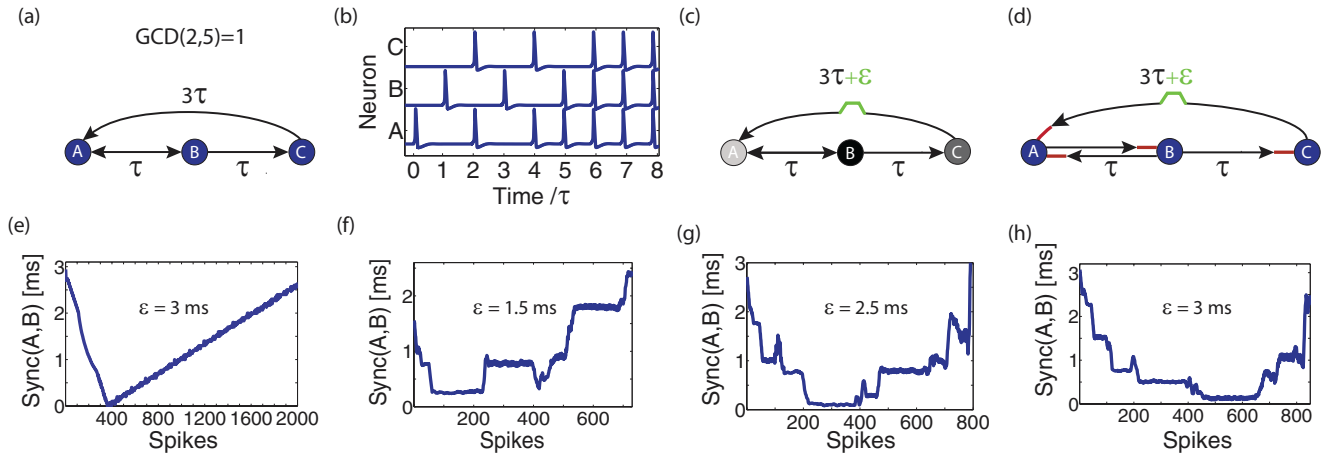

FIG. 3. (Color online) (a) Schematic of a heterogeneous neuronal circuit consisting of three neurons and bidirectional delay τ between neurons A and B and unidirectional delays τ and 3τ from neuron B to C and from C to A, respectively. The circuit consists of two delay loops, 2τ and 5τ, and ZLS as GCD(2,5) = 1. Neurons that fire together in the synchronous activity are represented by the same color. (b) Simulations of neuronal circuit 3(a) composed of HH neurons with $\tau = 30$ ms. The dynamics is initiated by a stimulation to neuron A. ZLS emerges after a transient of 7τ ms. (c) Schematic of the neuronal circuit 3(a), but the 3τ delay from neuron C to A is extended by ε. Neurons are colored differently since ZLS is not a solution. (d) Schematic of the effective extension of each delay, illustrated by the appended red thicker bar. ZLS is temporarily restored, represented by the same color for the three neurons. (e) The time lag between the evoked spikes of neurons A and B is presented as a function of the number of spike pairs obtained from simulations of circuit 3(d) with $\varepsilon = 3$ ms. After a neuron evoked spike, similar to 2(b), its incoming delays are stretched by $\Delta = 0.004$ ms. Artificially ignoring spikes arriving at a neuron in a refractory period of 4 ms, ZLS is restored after ~400 spike pairs in accordance with Eq. (2). (f)–(h) Experimental results of the time lag between neurons A and B as a function of spikes for neuronal circuit 3(d) initiated by an electrical stimulation to neuron A with $\varepsilon = 1.5$, 2.5, and 3 ms and $\tau = 80$ ms. Results are averaged over sliding windows of ten spikes.

artificially ignoring a second spike arriving at a neuron in a refractory period of 4 ms indicated that indeed the time lag between the evoked spikes of neurons A and B decay linearly to zero after $q \sim 3/(2 \times 0.004) = 375$ spikes per neuron [Eq. (3)] and is followed by desynchronization [Fig. 3(e)]. Experimental results with $\varepsilon = 1.5$, 2.5, and 3 ms and $\tau = 80$ ms indicated that the variable ε functions as a timer where the transient time to achieve synchronization increases with ε [Figs. 3(f)–3(h)]. The noisy quantized behavior is an outcome of the experimental time resolution, 0.5 ms in the timing of stimulations and 1/16 ms in the identification of evoked spikes, as is evidenced by the large fluctuations around the edges of the latency "stairs" [Figs. 3(f)–1(h)].

The quantity at the basis of this timer is the stretching of a loop per unit delay τ and per spike for each one of the neurons, ΔL. For the circuit Fig. 3(a), the shorter loop (2τ) consists of two neurons and $\Delta L_2 = 2\Delta/2 = \Delta$, whereas the longer loop (5τ) consists of only three neurons $DL_5 = 3D/5$ [see also Eq. (2)]. Hence, the relative stretching of the shorter loop is faster and compensates for the initial redundancy ε of the longer loop. The ratio 2:5 is restored and synchronization is achieved.

B. Second timer—stationary synchronization

The inverse scenario, leading to another type of timer, is shown by the heterogeneous circuit with five neurons and two loops, 4τ and 6τ [Fig. 4(a)]. Since GCD(4,6) = 2, the neuronal activity relaxes into two neuronal clusters, (A,B,D) and (C,E), where each neuronal cluster is in ZLS. Simulations of the neuronal circuit composed of Hodgkin-Huxley neurons confirm that after a transient of 9τ, two clusters are formed [Fig. 4(b)]. A modified circuit with 4τ and 6τ–ε loops does not maintain ZLS between neurons A and B [Fig. 4(c)]. After a neuron evokes q spikes, its incoming unidirectional delays elongate by $q\Delta$ as represented by the red thicker bars [Fig. 4(d)]. The restored ratio 4:6 between the two loops is given by the equation

$$\frac{4\tau + 2q\Delta}{4} = \frac{6\tau - \varepsilon + 5q\Delta}{6}, \tag{4}$$

which results in

$$q = \frac{\varepsilon}{2\Delta}. \tag{5}$$

Since the firing period of each neuron is GCD $\times$ $\tau = 2\tau$ [Fig. 4(b)], the restored duration of ZLS is $2q\tau$. Simulations with $\Delta = 0.004$ ms, $\varepsilon = 3$, and ignoring spikes in a refractory period of 4 ms indicate that $q \sim 3/(2 \times 0.004) = 375$ spikes [Fig. 4(e)]. Experimental results qualitatively with $\varepsilon =$ 3 ms and $\tau = 60$ ms indicate that ZLS is achieved in a shorter duration, $q \sim 200$ spikes [Fig. 4(f)]. Although results are qualitatively the same, the sources for the differences between simulations and experimental results are discussed in the next section.

The prominent feature of this timer is that after a transient trajectory, synchronization appears as a *stationary* phenomenon [Figs. 4(e) and 4(f)], unlike the *momentary* synchronous activity of the first timer [Figs. 3(e)–3(h)].

The emergence of ZLS in the two types of timers is clear since at some point of the dynamics $\varepsilon = 0$. Nevertheless, it is important to note that these two types of timers are not an outcome of their different GCD, but rather are originated from

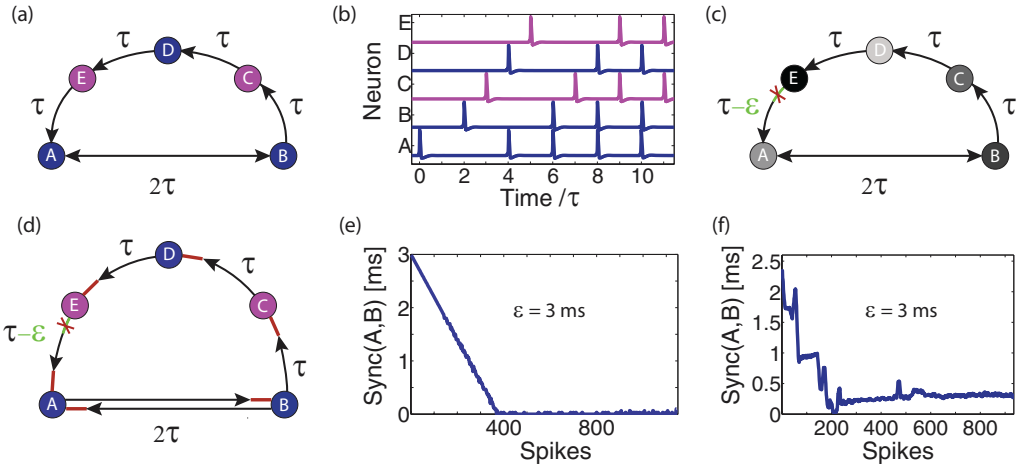

FIG. 4. (Color online) (a) Schematic of a heterogeneous neuronal circuit consisting of five neurons with 4τ and 6τ delay loops, and GCD(4,6) = 2 neuronal clusters, each in ZLS and represented by the same color. (b) Simulations of circuit 4(a) composed of HH neurons with $\tau = 50$ ms. The dynamics is initiated by a stimulation to neuron A. The synchronous activity of the 2-cluster emerges after a transient of 9τ ms. (c) Schematic of circuit 4(a), but the τ delay from neuron E to A is shortened by ε (represented by the red $\times$). Neurons are not synchronized and are colored differently. (d) Schematicof the effective stretching is illustrated by the appended red thicker bar for each directed delay. (e) The time lag between neurons A and B is presented as a function of spikes for simulations of circuit 4(d), where after a neuron evokes a spike its incoming delays are stretched by $\Delta = 0.004$ ms, $\varepsilon = 3$ ms and spikes arriving at a neuron in a refractory period of 4 ms are ignored. (f) Experimental results of the time lag between neurons A and B as a function of spikes for neuronal circuit 4(d) initiated by an electrical stimulation to neuron A with $\varepsilon = 3$ ms and $\tau = 60$ ms as in Fig. 3(f).

their intrinsic structures. In the following we sketch the critical dynamical periods of the two timers.

For the first timer [Fig. 3(a)] when ZLS first emerges neurons A and B fire simultaneously. Now neuron A receives two evoked spikes via two 4τ delay routes, B→C→A and A→B→A→B→A. The first route is comprised of 3 neurons whereas the second route is comprised of 5 neurons. Hence, the expansion of the second route is relatively larger, since it is comprised of a larger number of increase in neuronal response latencies. Consequently its spike falls into the refractory period of the first route, B→C→A, and practically the circuit degenerates into a directed *heterogeneous* loop, A→B→C→A. Synchronous activity cannot be maintained since the stretching of the loop is inhomogeneous.

For the second timer, the first moment where two neuronal clusters emerge [Figs. 4(a) and 4(b)], neuron A receives two evoked spikes via two 4τ delay routes, A→B→A and B→C→D→E→A. As the dynamics evolves, the first route becomes relatively shorter since its expansion is comprised of only two latencies, whereas the second route is comprise of five latencies. Hence, a spike absorbed via the second route falls into the refractory period from the spike that arrived earlier via the first route. Practically, the route B→C→D→E→A can be ignored and the circuit degenerates into two face-to-face (A↔B) neurons and synchronous activity can be maintained.

IV. EXPERIMETAL LIMITATIONS

Our multielectrode array system (MEA-1060; see also Methods section) consists of only one stimulator which can simultaneously stimulate several electrodes. Nevertheless, the time gap between consecutive stimulations is limited to ~20 ms. This limitation excludes the possibility to observe in our experiments the emergence of ZLS on a time scale of several milliseconds. In order to overcome this difficulty we shifted some of the neurons along the circuit delays such that ZLS is now mapped onto shifted ZLS characterized by a time lag between the evoked spikes of any pair of neurons.

The first timer, heterogeneous neuronal circuit 5(a), consists of three neurons with two delay loops, 2τ and $5\tau + \varepsilon$. An equivalent schematic circuit is depicted in Fig. 5(b). To overcome the above-mentioned experimental limitation neurons B and C were shifted. For the sake of clarity, the original neurons of circuit 5(a) and 5(b) before shifting are presented as small blue nodes in their original location. The three large gray nodes represent the actual location of the neurons in the experimental circuit with the corresponding delays among themselves [Fig. 5(d)]. Note that the blue node B is plotted twice, since it participates in two drives, independent delays, to nodes A and C. At ZLS the blue neurons fire simultaneously, hence gray node B fires 0.3τ before blue node B and gray node C fires 0.4τ after blue node C. The relative timings of the spikes measured in the experiment, Figs. 3(f)–3(h), on the gray neurons are shifted to the original blue neurons.

The neuronal response latencies of the three neurons (L_A, L_B, L_C) at a stimulation rate of 12.5 Hz are presented in Figs. 6(a)–6(c) as a function of the number of evoked spikes. Failures, stimulations without evoked spikes, were not counted. The initial latencies of the neurons, estimated from the first few spikes, were subtracted from the incoming delays for each one of the neurons. For instance, the initial latency of neuron B (~6 ms) was subtracted from the 0.7τ incoming delay from neuron A.

The quantity at the basis of this timer is the stretching of each one of the neurons per spike, and the stretching of a loop per unit delay τ, ΔL. The stretching of the 2τ loop, $\Delta L_2 = (L_A + L_B)/2$, is presented by the blue line in Fig. 6(d), whereas

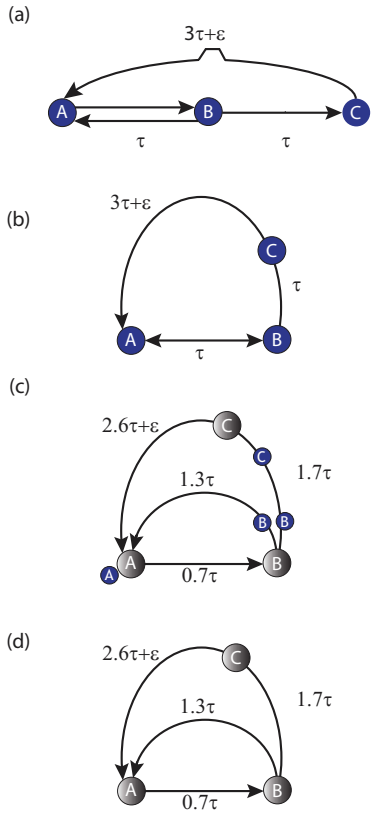

FIG. 5. (Color online) Schematic of the shifted ZLS for the first timer (Fig. 3) as explained in the text.

the stretching of the $\sim 5\tau$ loop, $\Delta L_5 = (L_A + L_B + L_C)/5$, is presented by the red line in Fig. 6(d). The experimental results of the difference between the relative stretching of the two loops $\Delta L_{2,5} = (L_A + L_B)/2 - (L_A + L_B + L_C)/5$ are presented in Fig. 6(e). Results indicate that indeed the relative stretching of the short loop is larger than for the longer loop [Figs. 6(d) and 6(e)]. Nevertheless, the difference does not increase linearly with the number of evoked spikes, since there is a variance among the profiles of the neuronal response latencies where each one of them does not scale linearly with the number of evoked spikes [Figs. 6(a)–6(c)]. The cusp in both blue and red lines in Fig. 6(d) around 1000 spikes is attributed to the emergence of the intermittent phase of neurons A and C.

A schematic of shifted ZLS for the second timer, heterogeneous neuronal circuit 4(a), is presented in Fig. 7. For the sake of clarity, the original five neurons of circuit 7(a) before shifting are presented in Fig. 7(c) as small nodes in their original location and color. The five large gray nodes represent the experimental circuit and the actual delays among connecting neurons [Fig. 7(d)]. As a result, gray node B fires 1.2τ after blue node B, gray node C fires 0.6τ after purple node C, gray node D fires 0.4τ after blue node D, and gray node E fires 0.2τ before purple node E. The relative timings of the spikes measured in the experiment on the gray neurons [Fig. 4(f)] are shifted to the original blue and purple neurons.

The neuronal response latencies of the five neurons $(L_A, L_B, L_C, L_D, L_E)$ at a stimulation rate of 12.5 Hz are presented in Figs. 8(a)–8(e) as a function of the number of evoked spikes. Failures, stimulations without evoked spikes, were not counted. The initial latencies of the neurons, estimated from the first few spikes, were subtracted from the incoming delays for each one of the neurons. For instance, the initial latency of neuron A ($\sim$3 ms) was subtracted from the 0.8τ incoming delay from neuron B and from the $1.2\tau - \varepsilon$ delay coming from neuron E. Experimental results Fig. 4(f) indicate that the emergence of shifted ZLS is robust to nonidentical profiles (mostly concave) of the five neuronal response latencies. Actually, the emergence of ZLS is controlled by the relative stretching of the two loops $\Delta L_{4,6} = (L_A + L_B + L_C + L_D + L_E)/6 - (L_A + L_B)/4$ [Fig. 8(f)].

The two types of timers [Figs. 5(a) and 7(a)] depict experimentally synchronous activity with coordinated mismatches of $\sim$1–3 ms over synaptic delays of $\sim$80–100 ms, where such slightly relatively imprecise delays still represent inflexible prerequisite biological conditions. Furthermore,

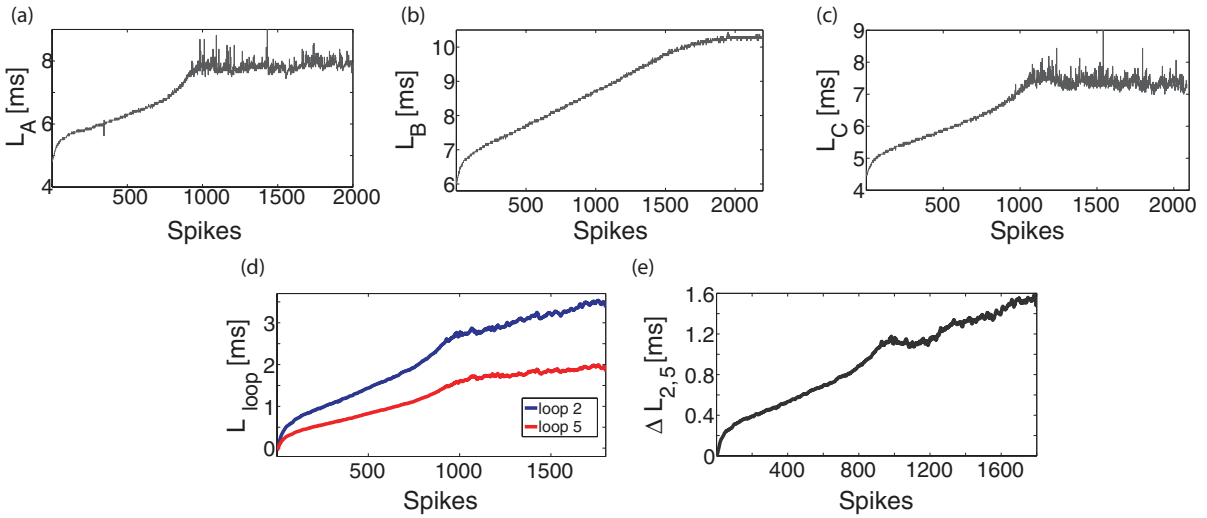

FIG. 6. (Color online) (a)–(c) Neuronal response latencies (L_A, L_B, L_C) of the three neurons used in the experiment [Figs. 3(f)–3(h)]. (d) The experimental elongation of the two circuit loops per unit delay, τ, as a function of spikes: $\Delta L_2 = (L_A + L_B)/2$ and $\Delta L_5 = (L_A + L_B + L_C)/5$. (e) The difference between the relative elongation of the two circuit loops $\Delta L_{2,5} = (L_A + L_B)/2 - (L_A + L_B + L_C)/5$ as a function of spikes.

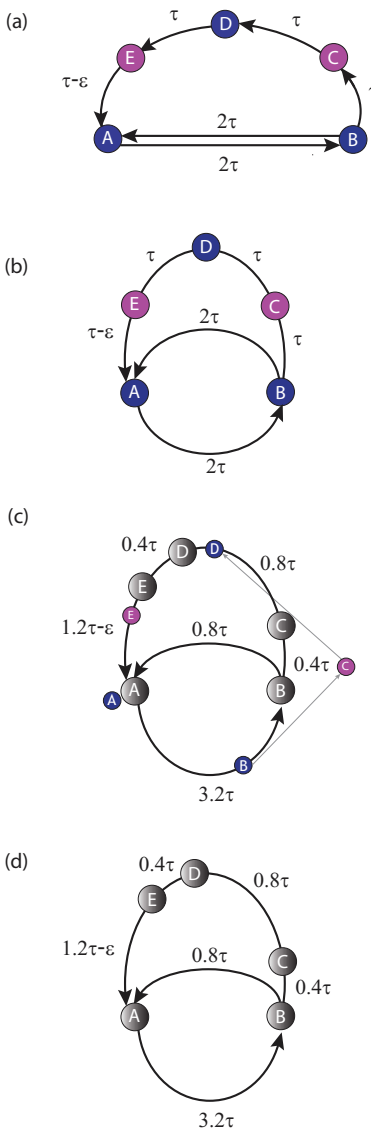

FIG. 7. (Color online) Schematic of the shifted ZLS for the second timer (Fig. 4) as explained in the text.

transient periods to synchronous activity of a few hundreds of τ ms are also beyond the typical cortical response time scale. Producing much shorter delays which are relevant to cortical dynamics as well as monitoring circuits composed of much larger numbers of neurons are currently beyond our experimental capabilities. Nevertheless, these types of neuronal circuits are scalable, where the stretching of synfire chains [3] (loops) increases linearly with the number of their relays. Figure 9 depicts a schematic of heterogeneous neuronal circuit 3(a) with two additional neurons (light blue) on the delay route from A to B. The circuit consists of five neurons while the total delay loops remain unchanged, 2τ and $5\tau + \varepsilon$, and ZLS is reached as GCD(2,5) = 1 with $\varepsilon = 0$. Simulation results of this circuit composed of Hodgkin-Huxley neurons are presented in Figs. 9(b) and 9(c) with $\varepsilon = 3$ and 6 ms, respectively. The time lag between the evoked spikes of neurons A and B is presented as a function of the counted spike pairs obtained in the simulation. After a neuron evoked a spike its incoming delays are stretched by $\Delta = 0.004$ ms ($4\ \mu$s) and spikes arriving at a neuron in a refractory period of 4 ms are ignored. ZLS is temporarily restored after ~130 and ~250 spike pairs for $\varepsilon = 3$ and 6 ms, respectively. These transients are in accordance with $q = 150$, $q = 300$ spikes obtained from the equation to restore the ratio 2:5 between the two loops,

$$\frac{2\tau + 4q\Delta}{2} = \frac{5\tau + \varepsilon + 5q\Delta}{5}, \tag{6}$$

results in

$$q = \frac{\varepsilon}{5\Delta}. \tag{7}$$

This equation has to be compared with Eq. (3), without neurons D and E, where ZLS is achieved for $q \sim 400$, since $q = \varepsilon/2\Delta$ only. The addition of two neurons improves the stretchability of the two neuronal circuit loops; however, the relative elongation of the shorter loop (2τ) is enhanced further. This feature leads to a shorter transient time to achieve temporary ZLS.

Another factor which will decrease the transient time to achieve synchronous activity is the fast increase in the neuronal response latency in the initial spiking activity (see, for instance, Figs. 6 and 8). Both of these effects, long synfire chains (loops) and initial fast increase in the neuronal response latencies, are expected to significantly shorten the transient to synchronization.

V. SIMULATIONS OF CIRCUITS COMPOSED OF HODGKIN-HUXLEY NEURONS

A. Parameters used for the Hodgkin-Huxley model

To explore the local and nonlocal behavior of cortical neural activity, exemplified in Figs. 3(a), 3(b), 3(e), 4(a), 4(b), and 4(e), a realistic numerical model was designed in which the dynamic behavior of a solitary neuron, delays, and connectivity strength were taken into account [9,10]. Each neural cell was simulated using the well-known Hodgkin-Huxley model [23] (HH).

For every neuron (i) in the network the membrane potential V^i is described by the following differential equation:

$$C_m \frac{dV^i}{dt} = -g_{\mathrm{Na}} m^{i^3} h^i (V^i - E_{\mathrm{Na}}) - g_k n^{i^4} (V^i - E_k) - g_L (V^i - E_L) + I^i_{\mathrm{syn}} + I^i_{\mathrm{ext}} + I^i_{\mathrm{noise}}, \tag{8}$$

where $C_m = 1\ \mu\mathrm{F/cm}^2$ is the membrane capacitance. The constants $g_{\mathrm{Na}} = 120$ ms/cm^2, $g_k = 36$ ms/cm^2, and $g_L = 0.3$ ms/cm^2 are the maximal conductances of their corresponding channels, and $E_{\mathrm{Na}} = 50$ mV, $E_k = -77$ mV, and $E_L = -54.5$ mV are the corresponding reversal potentials. I^i_{syn} is the synaptic current, I^i_{ext} is the initial external stimulation given to one of the neurons in order to activate the neural circuit, and I^i_{noise} is the background noise (not taken into account in the present study). The voltage-gated ion channels m, n, and h represent the activation and inactivation of the sodium and potassium channels and can be described by the following three differential equations, where X stands for m, n, h:

$$\frac{dX^i}{dt} = \alpha^i_X(V^i)(1 - X^i) - \beta^i_X(V^i)X^i. \tag{9}$$

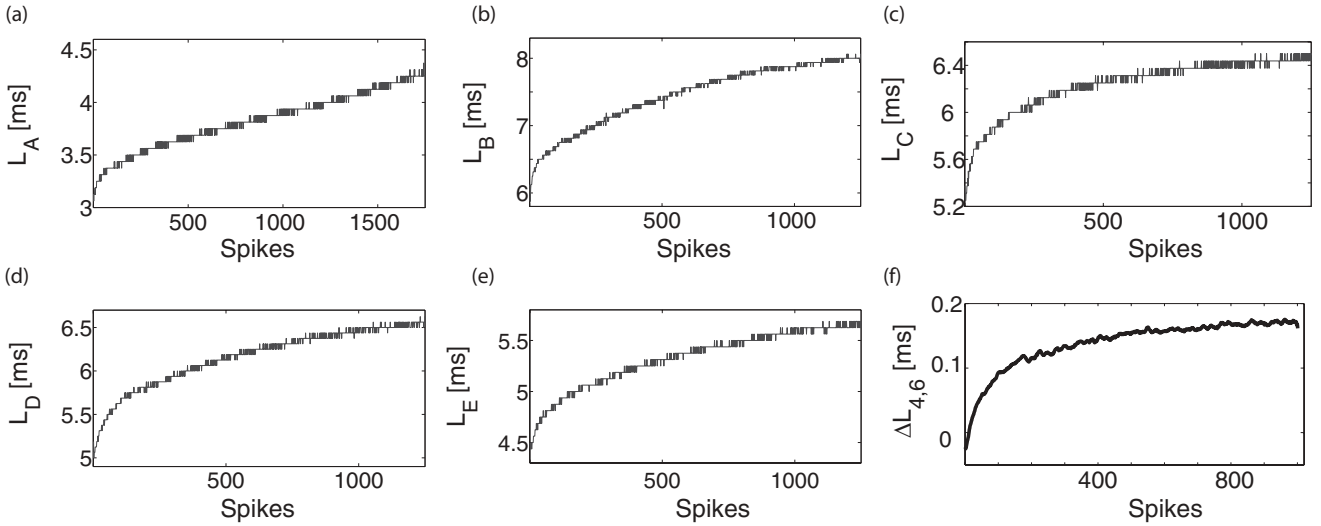

FIG. 8. (a)–(e) Neuronal response latencies (L_A, L_B, L_C, L_D, L_E) of the five neurons used in the experiment [Figs. 7(d) and 4(f)]. (f) Experimental results of the difference between the relative stretching of the two circuit loops $\Delta L_{4,6} = (L_A + L_B + L_C + L_D + L_E)/6 - (L_A + L_B)/4$ as a function of spikes [Eq. (4)].

The experimentally fitted voltage-dependent transition rates are

$$\begin{aligned}
\alpha_m(V) &= \frac{0.1(V+40)}{1-\exp[-0.1(V+40)]},\\
\beta_m(V) &= 4\exp(-V+65/18),\\
\alpha_n(V) &= \frac{0.01(V+55)}{1-\exp[-0.1(V+55)]},\\
\beta_n(V) &= 0.125\exp(-V+65/80),\\
\alpha_h(V) &= 0.07\exp(-V+65/20),\\
\beta_h(V) &= \frac{1}{1+\exp[-0.1(V+35)]}.
\end{aligned} \tag{10}$$

In the absence of any type of noise or synaptic influence on the neuron, the steady state $V^i_{\text{rest}} = -65$ mV is stable for $I_{\text{ext}} < 9.78\,\mu\text{A/cm}^2$. However, when $9.78 < I_{\text{ext}} < 154.5\,\mu\text{A/cm}^2$ the HH neuron starts to fire periodically [4]. Our simulations were adjusted to imitate the behavior of a random biological neural cell.

The synaptic transmission between neurons is modeled by a postsynaptic conductance change with the form of an α function:

$$\alpha(t) = \frac{\exp(-t/\tau_d) - \exp(-t/\tau_r)}{\tau_d - \tau_r}, \tag{11}$$

where the parameters $\tau_d = 10$ ms and $\tau_r = 1$ ms stand for the decay and rise time of the function and determine the duration of the response. The synaptic current $I^i_{\text{syn}}(t)$ takes the form

$$I^i_{\text{syn}}(t) = -g_{\max}\sum_j \sum_{t_j^{sp}} \alpha\big(t - t_j^{sp} - \delta_{ij}\big)(V - E_{\text{syn}}). \tag{12}$$

Here, {j} is the group of neurons coupled to neuron i. The internal sum is taken over the train of presynaptic spikes occurring at t_j^{sp} of a neuron j in the group. All nodes were excitatory, and were differentiated from inhibitory transmissions by setting the synaptic reversal potential to be $E_{\text{syn}} = 0$ mV instead of $E_{\text{syn}} = -80$ mV. $g_{\max} = 1.2$ ms/cm^2 describes the maximal synaptic conductance between neurons i and j. The set of differential

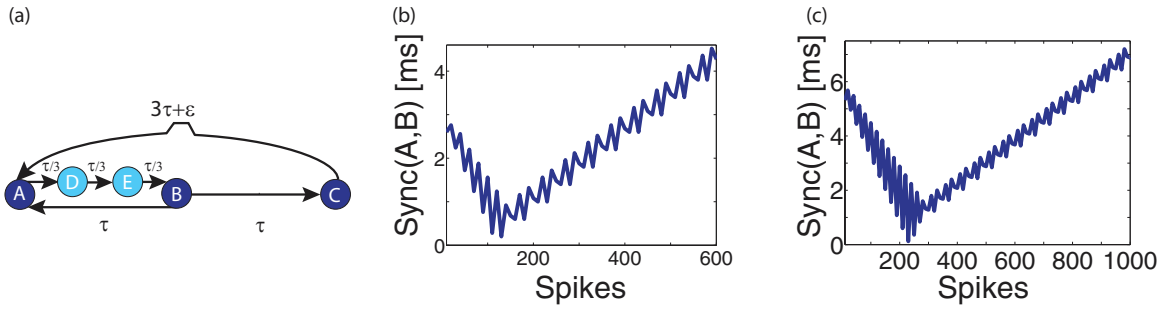

FIG. 9. (Color online) Enhanced stretchability exemplified by simulations with longer synfire chains. (a) Schematic of heterogeneous neuronal circuit 3(a) [see Fig. 3] with two additional neurons (light blue) on the delay route from A to B. The circuit consists of five neurons while the total delay loops remain unchanged, 2τ and $5\tau + \varepsilon$. (b), (c) The time lag between the evoked spikes of neurons A and B is presented as a function of the counted spike pairs obtained from simulations of circuit 3(a) composed of HH neurons with $\varepsilon = 3$ ms (b) and 6 ms (c). After a neuron evoked spike, its incoming delays are stretched by $\Delta = 0.004$ ms (4 μs) and spikes arriving at a neuron in a refractory period of 4 ms are ignored.

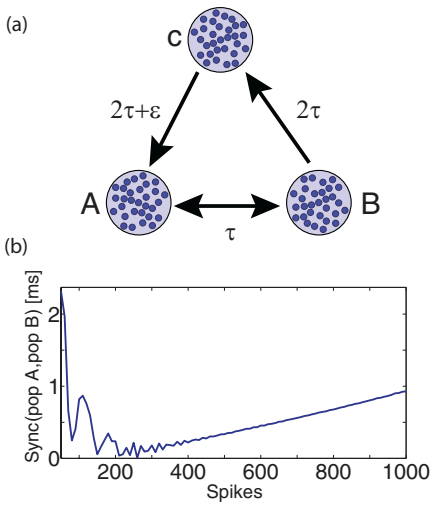

FIG. 10. (Color online) (a) Schematic of a heterogeneous neuronal circuit consisting of three nodes with two delay loops, 2τ and $5\tau+\varepsilon$, and with $\varepsilon = 0$ ZLS achieved as GCD(2,5) = 1. Each one of the three nodes is comprised of 30 excitatory Hodgkin-Huxley neurons. A connection between neurons belonging to two connecting nodes is excitatory only and selected with a probability of $p_{\text{out}} = 0.2$, and the delay between them was taken from a uniform distribution in the range $[\tau-1, \tau+1]$ ms, where τ was selected to be 30 ms. (b) The time lag between evoked spikes of populations A and B is presented as a function of counted population spike pairs for initial $\varepsilon = 3$ ms. After a neuron evokes a spike, its incoming delays are stretched by $\Delta = 0.004$ ms.

equations were integrated numerically using Heun's method. The time step of the integration was 0.002 ms.

B. Population dynamics—the Hodgkin-Huxley model

In a set of simulation studies at the population dynamics (cell assembly) level we demonstrated that the cortical timers remain valid, and the circuit activity becomes less sensitive to fluctuations [9].

Schematic of a heterogeneous neuronal circuit consisting of three nodes with two delay loops, 2τ and $5\tau+\varepsilon$, is presented in Fig. 10. For $\varepsilon = 0$ ZLS is achieved as GCD(2,5) = 1. Each node represents one cortical patch comprised of N neurons. Every neural cell was simulated using the HH model and in terms of biological properties it was assumed that distant cortico-cortical connections are (almost) exclusively excitatory [3]. In this framework, cortical areas are connected reciprocally across the two hemispheres and within a single hemisphere [26,27], where small functional cortical units (patches) connect to other cortical patches in a pseudorandom manner. The number of patches to which a single patch connects varies considerably, where typically, it grows as the square root of the number of cortical neurons [28] resulting for a mouse in 3 to 6 [29], and most likely for humans in roughly 150.

Each one of the three nodes in our simulations is comprised of 30 excitatory Hodgkin-Huxley neurons. A connection between neurons belonging to different nodes was excitatory only and was selected with a probability of $p_{\text{out}} = 0.2$. The delay τ_{ij} between a pair of neurons, belonging to different nodes i and j, represents the time it takes an action potential to travel through the axon from the presynaptic neuron i to the postsynaptic neuron j and was taken from a uniform distribution in the range $[\tau-1, \tau+1]$ ms, where τ was selected to be 30 ms. Figure 10(b) presents the time lag between evoked spikes of populations A and B as a function of counted population spike pairs for the case of $\varepsilon = 3$ ms. Note that a population spike is calculated as the average over the spike timing of all neurons comprising the population. After a neuron evoked spike, its incoming delays are stretched by $\tau = 0.004$ ms. One can easily verify that ZLS is unstable for $\varepsilon < 0$, hence this neuronal circuit belongs to the class of the first timer (Fig. 3). Simulations indicate that indeed ZLS is temporarily restored after ~200 spikes [Fig. 10(b)].

The robustness of our neuronal timers to population dynamics is especially crucial to the realization of shorter neuronal delay loops, where the activity of a single neuron will stop spontaneously due to the relative neuronal refractory period or synaptic fatigue.

VI. METHODS

Cell preparation. Cortical neurons were obtained from newborn rats (Sprague-Dawley) within 48 h after birth using mechanical and enzymatic procedures described in an earlier study [20]. Rats were euthanized by CO_2 treatment according to protocols approved by the National Institutes of Health. The neurons were plated directly onto substrate-integrated multielectrode arrays and allowed to develop functionally and structurally mature networks over a time period of 2–3 weeks. The number of plated neurons in a typical network is on the order of 1,300,000, covering an area of about 380 mm^2. The preparations were bathed in minimal essential medium supplemented with heat-inactivated horse serum (5%), glutamine (0.5 mM), glucose (20 mM), and gentamicin (10 g/ml), and maintained in an atmosphere of 37 °C, 5% CO_2, and 95% air in an incubator as well as during the recording phases.

All experiments were conducted in the standard growth medium, supplemented with 5 μM Bicuculline, 10 μM CNQX (6-cyano-7-nitroquinoxaline-2,3-dione), and 80 μM APV (amino-5-phosphonovaleric acid); this cocktail of synaptic blockers made the spontaneous network activity sparse. At least 1 h was allowed for stabilization of the effect.

Measurements and stimulation. An array of 60 Ti/Au/TiN extracellular electrodes, 30 μm in diameter, and spaced either 500 or 200 μm from each other (Multi-ChannelSystems, Reutlingen, Germany) were used. The insulation layer (silicon nitride) was pretreated with polyethyleneimine (Sigma, 0.01% in 0.1M borate buffer solution). A commercial amplifier (MEA-1060-inv-BC, MCS, Reutlingen, Germany) with frequency limits of 150–3000 Hz and a gain of $\times$1024 was used. Monophasic square voltage pulses (100–500 μs, 100–900 mV) were applied through extracellular electrodes. The data were digitized using a data acquisition board (PD2-MF-64-3M/12H,UEI, Walpole, MA). Each channel was sampled at a frequency of 16 K samples/s. Action potentials were detected on-line by threshold crossing. Data processing and conditioned stimulation were performed using SIMULINK (The Mathworks, Natick, MA) based xPC target application.

Cell selection. Each circuit node was represented by a stimulation source (source electrode) and a target for the

stimulation—the recorded electrode (target electrode). The stimulation electrodes (source and target) were selected as the ones that evoked well-isolated and well-formed spikes and a reliable response with a high signal-to-noise ratio. This examination was done with a stimulus intensity of 800 mV, after 30 repetitions at a frequency of 5 Hz.

Stimulation control. The activity of all target electrodes for each stimulation was collected and entailed stimuli were delivered in accordance to the adjacency matrix.

VII. CONCLUSIONS

We presented theoretical evidence which we have corroborated experimentally to show how the apparent variability in brain building blocks can turn into an advantage. We showed that the unavoidable increase in neuronal response latency, for instance, to ongoing stimulation acts as a nonuniform gradual stretching of neuronal circuit delay loops. This apparent nuisance is revealed to be an essential mechanism to achieve various types of neuronal timers, where synchronization emerges without predefined precisely matched synaptic delays. These findings emerged from an experimental procedure where *conditioned stimulations* were enforced on a circuit of neurons embedded within a large-scale network of cortical cells *in vitro*, and were corroborated and extended by simulations of circuits composed of Hodgkin-Huxley neurons with time-dependent latencies. These findings announce a cortical time scale for timers based on tens of microseconds stretching of neuronal circuit delay loops per spike. It is important to generalize our results to the limit where delays among neurons, neuronal latencies, and refractory periods all occur on a similar time scale.

ACKNOWLEDGMENTS

The authors thank Vladimir and Elleonora Lyakhov for invaluable technical assistance. The research has received funding from the European Union Seventh Framework Program FP7 under Grant agreement No. 269459 to S.M. and a grant of the Ministry of Science and Technology of the State of Israel and MATERA, Grant agreement No. 3-7878, to S.M.

[1] D. O. Hebb, *The Organization of Behavior: A Neuropsychological Theory* (Wiley, New York, 1949).
[2] G. Buzsaki, Neuron **68**, 362 (2010).
[3] M. Abeles, *Corticonics: Neural Circuits of the Cerebral Cortex* (Cambridge University Press, Cambridge, 1991).
[4] E. Zohary, M. N. Shadlen, and W. T. Newsome, Nature **370**, 140 (1994).
[5] E. Vaadia, I. Haalman, M. Abeles, H. Bergman, Y. Prut, H. Slovin, and A. Aertsen, Nature **373**, 515 (1995).
[6] C. M. Gray, P. Konig, A. K. Engel, and W. Singer, Nature **338**, 334 (1989).
[7] A. Viriyopase, I. Bojak, M. Zeitler, and S. Gielen, Front. Comput. Neurosci. **6**, 49 (2012).
[8] M. N. Woodman and C. C. Canavier, J. Comput. Neurosci. **31**, 401 (2011).
[9] I. Kanter, E. Kopelowitz, R. Vardi, M. Zigzag, W. Kinzel, M. Abeles, and D. Cohen, Europhys. Lett. **93**, 66001 (2011).
[10] R. Vardi, A. Wallach, E. Kopelowitz, M. Abeles, S. Marom, and I. Kanter, Europhys. Lett. **97**, 66002 (2012).
[11] A. Riehle, S. Grün, M. Diesmann, and A. Aertsen, Science **278**, 1950 (1997).
[12] A. Kumar, S. Rotter, and A. Aertsen, Nat. Rev. Neurosci. **11**, 615 (2010).
[13] B. Ravoori, A. B. Cohen, J. Sun, A. E. Motter, T. E. Murphy, and R. Roy, Phys. Rev. Lett. **107**, 034102 (2011).
[14] M. Nixon, M. Fridman, E. Ronen, A. A. Friesem, N. Davidson, and I. Kanter, Phys. Rev. Lett. **108**, 214101 (2012).
[15] Y. Aviad, I. Reidler, M. Zigzag, M. Rosenbluh, and I. Kanter, Opt. Express **20**, 4352 (2012).
[16] V. Flunkert, S. Yanchuk, T. Dahms, and E. Schoell, Phys. Rev. Lett. **105**, 254101 (2010).
[17] R. De Col, K. Messlinger, and R. W. Carr, J. Physiol. **586**, 1089 (2008).
[18] A. Gal, D. Eytan, A. Wallach, M. Sandler, J. Schiller, and S. Marom, J. Neurosci. **30**, 16332 (2010).
[19] D. Soudry and R. Meir, Front. Neurosci. **6**, 4 (2012).
[20] S. Marom and G. Shahaf, Q. Rev. Biophys. **35**, 63 (2002).
[21] J. P. Thivierge and P. Cisek, J. Neurosci. **28**, 7968 (2008).
[22] T. Tateno, Y. Jimbo, and H. P. C. Robinson, Neuroscience **134**, 425 (2005).
[23] A. L. Hodgkin and A. F. Huxley, J. Physiol. **117**, 500 (1952).
[24] I. Kanter, M. Zigzag, A. Englert, F. Geissler, and W. Kinzel, Europhys. Lett. **93**, 60003 (2011).
[25] R. Vardi, R. Timor, S. Marom, M. Abeles, and I. Kanter, Europhys. Lett. **100**, 48003 (2012).
[26] D. J. Felleman and E. Mcclendon, Invest. Ophthalmol. Visual Sci. **32**, 1036 (1991).
[27] J. W. Scannell, C. Blakemore, and M. P. Young, J. Neurosci. **15**, 1463 (1995).
[28] V. Braitenberg, J. Comput. Neurosci. **10**, 71 (2001).
[29] V. Braitenberg and A. Shuz, *Cortex: Statistics and Geometry of Neuronal Connectivity*, 2nd ed. ed (Springer, Berlin, 1998).